# A Three-Dimensional Model for Evaluating the Performance of Tubular-Shaped PEM by CFD Simulation[1]

**M. M. Sabzehmeidani[a], * and B. ZareNezhad[a]**

[a]*School of Chemical, Petroleum and Gas Engineering, Semnan University, Semnan, PO Box 35195-363 Iran*
***e-mail: m.sabzehmeidani@gmail.com***

**Abstract**—The CFD simulation of a tubular-shaped proton exchange membrane (PEM) fuel cell in the patterns co-current flow for evaluation of the effects of different influencing parameters on fuel cell performance is presented. The model considers transport phenomena in a fuel cell involving mass and momentum transfer, electrode kinetics, and potential fields. The governing equations coupled with the CFD model are then solved using the finite element method. The predicted cell potentials are in good agreement with the available experimental data. The parametric studies have been conducted to characterize the effects of the gas diffusion layer (GDL) porosity and length, the inlet velocity of gases, and the hydrogen channel diameter on various cell performance parameters such as the concentration of reactants/products and cell current densities. The effect of the length and diameter of the channel on cell current density and the optimum gas diffusion layer porosity at a given hydrogen channel diameter to obtain the maximum current density is determined. In this work, a systematic procedure to optimize PEM fuel cell gas channels in the systems bipolar plates with the aim of globally optimizing the overall system net power performance was carried out.

## INTRODUCTION

Fuel cells technology is attracting more consideration as one of the solutions to the energy and environmental problems [1−5]. Fuel cells are electrochemical energy converters that convert chemical energy of fuel into electrical energy. One kind of the fuel cells is called the proton exchange membrane (PEM) fuel cell that operates at a considerably lower temperature than other types of fuel cells. The PEM fuel cells are well-set and light weight and high power density and low environmental impact [6−8]. All of PEM fuel cell consists of three essential compartments: polymer electrolyte membrane, an anode and a cathode. At the anode a hydrogen is oxidized into electrons and protons, while at the cathode oxygen is reduced [9, 10]. In many cases, modelling efforts concentrate on the cathode electrode (gas diffusion layer plus catalyst layer) or the membrane electrode assembly (MEA) [11, 12].

The gas diffusion layers are used to increase the reaction region available by the gas reactants. These diffusion layers allow a spatial distribution on the around of membrane in both the path of bulk flow and the path of orthogonal flow but parallel to the membrane [13, 14]. Typically, gas diffusion layers are constructed with a thickness in the range of 100−300 μm. The gas diffusion layer also assists in water management by allowing an appropriate amount of water to reach, and be held at, the membrane for hydration [15]. The difficult experimental PEM of fuel cell systems has stimulated efforts to develop models that could simulate and predict multidimensional coupled transport of reactants and charged species using computational fluid dynamics (CFD) methods. Theoretical studies on simulation of PEM fuel cells have been carried out to enhance the efficiency of these apparatuses. All theoretical studies concentrate on electrochemical kinetics and transport phenomena of PEM fuel cells (PEMFCs).

Much research [16, 17] has been carried out on PEMFCs ranging from one-dimensional and two-dimensional models showing phenomena in a PEM fuel cell. Dutta et al. [14] obtained velocity, density and pressure contours in the gas diffusion layers. They used a finite volume technique for solving model equations. Their results illustrated that the current direction is drastically dependent on the mass transfer mechanism in the membrane−electrode assembly.

---

[1] The article is published in the original.

Air flow     Hydrogen flow     Air flow

Anode gas diffusion layer

Anode catalyst layer

Membrane

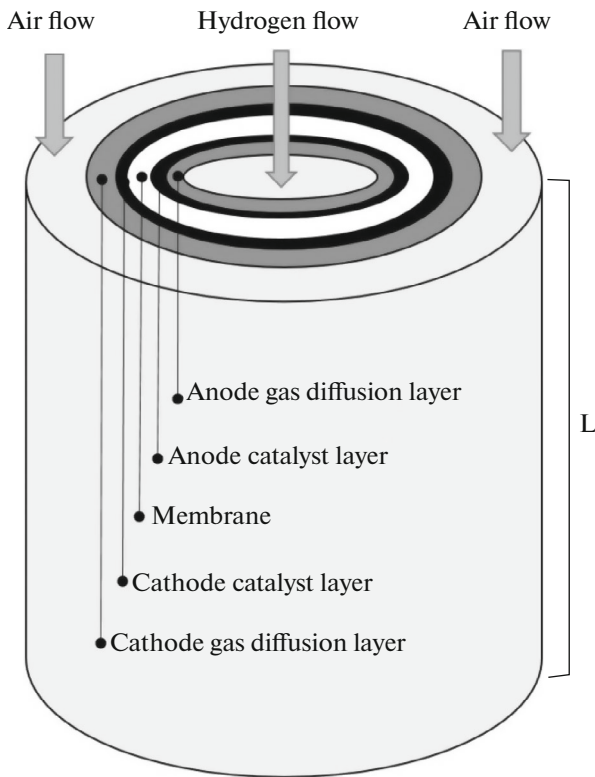Cathode catalyst layer

Cathode gas diffusion layer

L

**Fig. 1.** Geometry of a PEM fuel cell.

Futerko and Hsing [18] applied the finite element method (FEM) for solving governing equations in the gas diffusion layers and flow channels. They studied the resistance of membranes in polymer electrolyte fuel cells. Their modeling findings illustrated that the mole fraction of reactant gases, water content in the membrane and current density are dependent on pressure. More recently, Rodatz et al. [19] carried out studies on the operational aspects of a PEMFC stack under practical conditions. Their work focused exclusively on the pressure drop, two-phase flow and effect of bends. They noticed a decrease in the pressure drops at a reduced stack current. Ahmed and Sung [20] performed a numerical model to investigate the effects of channel geometrical configuration and shoulder width at high current density in the performance PEM fuel cell. Their result further reveals the presence of an optimum channel-shoulder ratio for optimal fuel cell performance. Al-Baghdadi [21] carried out the simulation of the tubular-shaped PEM fuel cell to investigate information about the transport phenomena inside the fuel cell such as reactant gas concentration distribution, temperature distribution, potential distribution in the membrane and gas diffusion layers, activation overpotential distribution, diffusion overpotential distribution, and local current density distribution. ZareNezhad and Sabzemeidani

[22] optimized flow channel dimensions using a 3-dimensional and isothermal model. They investigated the effect of channel dimensions on current density and hydrogen consumption in a fuel cell. They found that an increase in the flow velocity from 0.1 to 0.5 m/s leads to a decrease in the optimum channel width from 0.8 to 0.6 mm. The tubular-shaped fuel cell is one of the new architectures in PEM fuel cell. Fuel cell investigative institutes may have performed different experimental studies for tubular-shaped PEM fuel cell, but would be dedicated very limited information are accessible in the open access literature. There are various reasons that make the tubular architectures more useful than the planar fuel cell : lower pressure drop along the tubular fuel cell and uniform pressure in the cathode of MEA and the greater cathode area surface that increases the content of oxygen reduction and the reaction rate of oxygen reduction is very slow toward the reaction rate of hydrogen oxidation [21, 23]. In this paper, a single-phase and isothermal, fully three-dimensional CFD model of the quarter of tubular-shaped PEM fuel cell with the patterns co-current flow is presented. The model accounts for detailed species mass transport, potential losses in the gas diffusion layers and membrane, electrochemical kinetics. The full computational domain consists of cathode and anode gas flow fields, gas diffusion layers, catalyst layers, and a proton exchange membrane (Fig. 1). Also this model is used to study the effects of several material parameters and the effect of channel geometry on fuel cell performance and the optimal operating conditions at different flow conditions are investigated by CFD simulation.

## CFD MODELING

A 3-dimensional isothermal model is presented to account the mass, momentum and species balances in the flow channels, the gas diffusion layer (GDL), and the catalyst layers. Electrochemical equations in the catalyst layer and GDL parts of the fuel cell and membrane are also considered in the proposed model. Model assumptions consist of steady state condition, laminar flow regime, ideal gas behavior, single phase (gas phase), proton conductivity of membrane is fixed, the gas diffusion layer is isotropic, activation over potential is constant, the membrane is not permeable for reactant gases, isothermal operation.

**Gas flow fields.** In the channel of fuel cell, the the governing equations include conservation of mass and momentum as shown below:

$$\nabla(\rho.\vec{u}) = 0, \qquad (1)$$

$$\nabla[((\nabla\vec{u}) + (\nabla\vec{u})^T)] + \rho(\vec{u}.\nabla)\vec{u} + \nabla p = 0. \qquad (2)$$

The mass balance in channel is described by the divergence of the mass flux through diffusion and convection. The steady state mass transport equation can be written in the following expression for species $i$:

$$\nabla.\vec{j}_i + \rho(\vec{u}.\nabla)\omega_i = R_i, \qquad (3)$$

$$\vec{j}_i = -\left(\rho\omega_i \sum_k D_{ik}\left(\nabla x_k + \frac{1}{p_A}[(x_k - \omega_k)\nabla p_A]\right)\right), \quad (4)$$

where $D_{ik}$ is diffusivity of mixture that can be calculated using Maxwell–Stefan equations. The parameteris $\rho$ the overall mass density of the gas mixture obtained from the ideal gas law by

$$\rho = \frac{P}{RT}. \qquad (5)$$

**Gas diffusion layers.** In the gas layer of the fuel cell, the the governing equations include conservation of mass and momentum as shown below:

$$\nabla(\rho.\vec{u}) = 0, \qquad (6)$$

$$\nabla.\left[-p + \frac{\mu}{\varepsilon_p}((\nabla\vec{u}) + (\nabla\vec{u})^T)\right. \\ \left. - \frac{2\mu}{3\varepsilon_p}(\nabla\vec{u})\right] - \left(\frac{\mu}{k_{br}}\right)\vec{u} = 0. \qquad (7)$$

In order to account for the mass transport equation in porous media, the diffusivities are corrected using the Bruggemann correction:

$$D_{ik}^{\text{eff}} = \varepsilon^{1.5} D_{ik}. \qquad (8)$$

The potential distribution in the gas diffusion layers is governed by

$$\nabla.(\sigma_e^{\text{eff}}\nabla\phi_e) = 0.$$

Within porous media, electrical conductivity of electrode and membrane are estimated from the modified Brueggemann equation [24]:

$$\sigma_e^{\text{eff}} = \sigma_e \times \varepsilon_e^{1.5}. \qquad (9)$$

**Catalyst layers.** The catalyst layer is treated as a thin interface, where sink and source terms for the reactants are implemented:

$$\nabla(\rho.\vec{u}) = Q_{br}.$$

$$\nabla.\left[-p + \frac{\mu}{\varepsilon_p}((\nabla\vec{u}) + (\nabla\vec{u})^T)\right. \\ \left. - \frac{2\mu}{3\varepsilon_p}(\nabla\vec{u})\right] - \left(\frac{\mu}{k_{br}} + \frac{Q_{br}}{\varepsilon_p^2}\right)\vec{u} = 0,$$

where $Q_{br}$ is source term in the catalyst layer due to reaction of reactant species and can be calculated from the following equation:

**Table 1.** Electrochemical reactions of sink term for water, hydrogen, and oxygen

| $O_2$ | $H_2$ | $H_2O$ |
|---|---|---|
| $\dfrac{i_v}{4F}$ | $-\dfrac{i_v}{2F}$ | $-\dfrac{i_v}{2F}$ |

$$Q_{br} = \sum_m \sum_i R_{i,m} M_i,$$

$R_{i,m}$ is the electrochemical reactions of hydrogen and oxygen and water in the catalyst layer:

$$R_{i,m} = \frac{\upsilon_{i,m} i_v}{n_m F}.$$

The electrochemical reactions of sink term for water and hydrogen and oxygen shown in Table 1.

The potential distribution in the catalyst layers is governed by

$$\nabla.(\sigma_e^{\text{eff}}\nabla\phi_e) = \pm i_{v,\text{total}}.$$

The source term, $i_{v,\text{total}}$ is given by

$$i_{v,\text{total}} = \sum_m a_v i_{\text{loc}}. \qquad (10)$$

The current densities, $i_{loc}$ are calculated using the Butler–Volmer equation in anode and in cathode:

$$i_a = i_{0,a}\left(\frac{Y_{H_2}}{Y_{H_2}^{\text{ref}}}\right)^{0.5} \\ \times \left(\exp\left(\frac{\alpha_{a,a}F\eta_{\text{act}}}{RT}\right) - \exp\left(\frac{-\alpha_{a,c}F\eta_{\text{act}}}{RT}\right)\right), \qquad (11)$$

$$i_c = i_{0,c}\left(\frac{Y_{O_2}}{Y_{O_2}^{\text{ref}}}\right) \\ \times \left(\exp\left(\frac{\alpha_{c,a}F\eta_{\text{act}}}{RT}\right) - \exp\left(\frac{-\alpha_{c,c}F\eta_{\text{act}}}{RT}\right)\right), \qquad (12)$$

where $i_{0,a}$ and $i_{0,c}$ are the exchange current density anode and cathode at a reference temperature (25°C) and pressure (1 atm), respectively. $\alpha_{a,a}$ and $\alpha_{a,c}$ are the anodic and the cathodic transfer coefficients for the reaction at the anode. $\alpha_{c,a}$ and $\alpha_{c,c}$ are the anodic and the cathodic transfer coefficients for the reaction at the cathode. $Y_{O_2}^{\text{ref}}$ and $Y_{H_2}^{\text{ref}}$ are the mass fractions for hydrogen and oxygen at a reference temperature (25°C) and pressure (1 atm), respectively. The values of the exchange current density and the transfer coefficients are listed from Siegel et al. [25]. $R$ is the universal gas constant (8.314 J mol$^{-1}$ K$^{-1}$), $F$ is Faraday constant (C mol$^{-1}$), and $T$ is the temperature (K). The activation over potential $\eta$ is given by

**Table 2.** Operational conditions used in the simulations of PEMFC

| Parameters | Value |
|---|---|
| Inlet anode/cathode temperature, °C | 80 |
| Inlet anode/cathode pressure, atm | 3 |
| Anode/cathode flow velocity, m/s | 2 |
| Relative humidity of inlet gases, % | 100 |
| Mole ratio of $O_2/N_2$ | 0.79/0.21 |
| Mass fraction of $H_2O$, anode | 0.7 |
| Mass fraction of $H_2$, anode | 0.3 |
| Mass fraction of $H_2O$, cathode | 0.14 |
| Mass fraction of $O_2$, cathode | 0.2 |
| Mass fraction of $N_2$, cathode | 0.66 |
| Inlet $O_2$ concentration, $kmol/m^3$ | 0.00086 |
| Inlet $H_2$ concentration, $kmol/m^3$ | 0.04 |

**Table 3.** Geometric parameters of the modeled fuel cell [8]

| Description | Value |
|---|---|
| Channel length, m | 0.005 |
| Hydrogen flow channel height (channel diameter), m | $1e^{-3}$ |
| Air flow channel height, m | $1e^{-3}$ |
| Gas diffusion layer thickness, m | $0.26e^{-3}$ |
| Wet membrane thickness (Nafion 117), m | $0.23e^{-3}$ |
| Catalyst layer thickness, m | $0.025e^{-3}$ |

$$\eta_{act} = \phi_s - \phi_l - E_{eq}. \qquad (13)$$

The relevant numerical and geometric parameters for this study are given in Tables 2 and 3.

**Boundary conditions.** The inlet values at the anode and cathode are determined for the velocity and species concentrations (Dirichlet boundary conditions). For all other variables, the gradient in the flow direction is assumed to be zero (Neumann boundary conditions). At the inlet, the velocity in the x-direction is determined to be $u = u_0$. At the inlet, the mass fraction is defined as $\omega = \omega_0$. At the walls no-slip boundary condition is applied. to the boundary velocity is zero in the case of a fixed wall $u = 0$. A mass insulation boundary condition is applied at the walls $-n.N_i = 0$. The outflow boundary condition is prescribed as $p = p_0$. The convective flux boundary condition is applied at the outlet.

## RESULTS AND DISCUSSION

The simulation results are compared with experimental data [26] in Fig. 2. The computed polarization curve values are in good agreement with the measured data in the range of current densities shown in the presented figure. As the main objective of this paper is to investigate the sensitivity of the fuel cell performance to the porosity and length of the GDL and the diameter of a tubular-shaped PEM fuel cell.

Reactant transport in the gas diffusion layer and catalyst layer has a significant impact on fuel cell performance. Within the GDL and catalyst layer, the reactant diffusive flux in the direction through the layer thickness is much more important than the flux in other directions. The wet reactant gases in the channel transport through the gas diffusion layer and attain the catalyst layer where the electrochemical reactions take place. Electrodes are considered as a porous media where reactant gases are distributed on the catalyst layers. The effect of the GDL porosity on the fuel cell performance was investigated at a constant channel length and different flow velocities that the shown in Fig. 3 were simulated. The current density increased gradually from at a porosity of 0.3 until an optimum was obtained at a porosity of 0.55 at different flow velocities. The reason is the increase in the hydrogen and oxygen gases through the gas diffusion layer to the reaction sites in catalyst layer, which increased the rate of reaction. The explanation is that the increase in the hydrogen and oxygen gases through the gas diffusion layer to the reaction sites in catalyst layer, that enhanced the rate of reaction.

Figure 4 illustrates the effect of changing the hydrogen channel diameter from 1.1 to 1.25 mm on the fuel cell performance at various GDL porosities from 0.3 to 0.65. The current density increased gradually from at a porosity of 0.3 until an optimum was obtained at a porosity of 0.55 at various hydrogen channel diameters. The reason is the increase in the pore space of the gas diffusion layer, which increases the transport of gases and enhance the reaction region accessible by reactants, on the other hand, the physical properties affecting transportation processes inside the gas diffusion layer.

Figure 5 illustrates the effect of changing the inlet velocity of gases from 1 to 2 m/s on the average mole fraction of $H_2$ at the outlet channel in the hydrogen channel diameter. When the inlet velocity of gases is
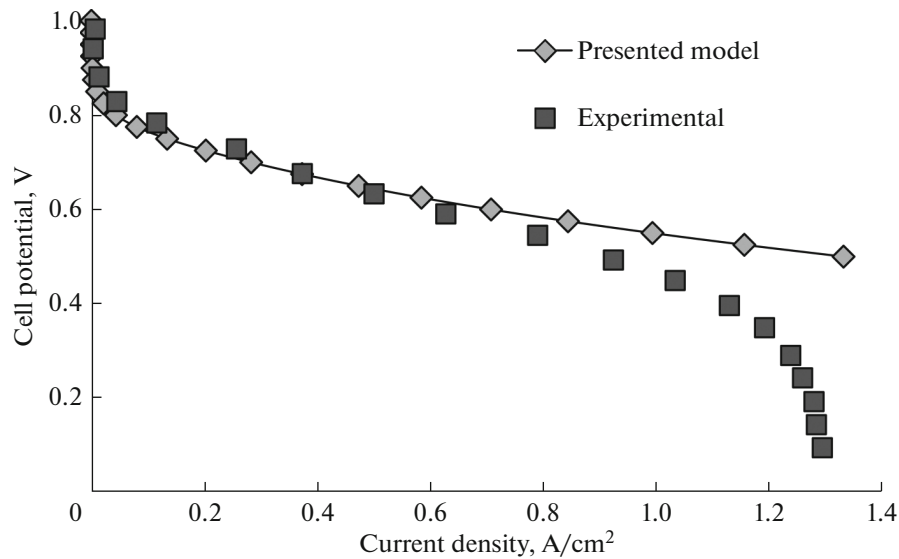
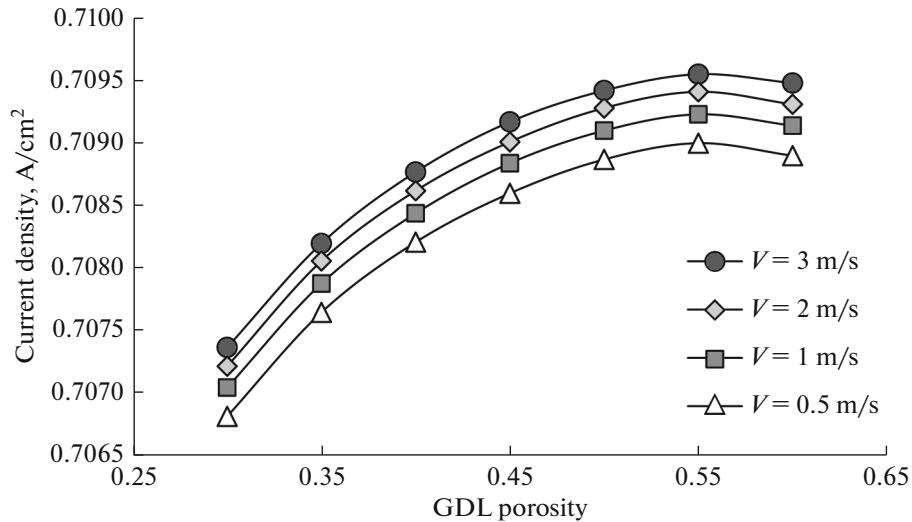**Fig. 2.** Comparison between the predicted and measured cell potentials.



**Fig. 3.** Effect of the GDL porosity on the current density at a cell potential of 0.6 V for different flow velocities.

increased, the average mole fraction of $H_2$ at the outlet channel is enhanced especially at lower hydrogen channel diameter. As observed, at the flow velocity 1 m/s, an increase in the hydrogen channel diameter from 0.25 to 1.75 mm leads to an increase in the average mole fraction of $H_2$ at the outlet channel.

The hydrogen molar fraction distribution in the anode side is shown in Fig. 6 for three various flow velocities. In general, the hydrogen molar fraction decreases during the anode side channel as it is being consumed and the decrease is small along the channel. The hydrogen molar fraction in the output channel

increases with an increase in the reactant gases flow velocities.

Figure 7 illustrates the distribution of velocity magnitude at a cell voltage of 0.6 V and confirm the mentioned details. Increasing in inlet velocity provides the reactant gases to the catalyst layers. Therefore, the efficiency of catalytic reaction enhances, and tubular-shaped PEM fuel cell performance improves.

Figure 8 illustrates the effect of the channel length of tube on the current density at a constant channel diameter for various flow velocities. The numerical results confirm that the current density decreased as the channel length of tubular-shaped PEM fuel cell is
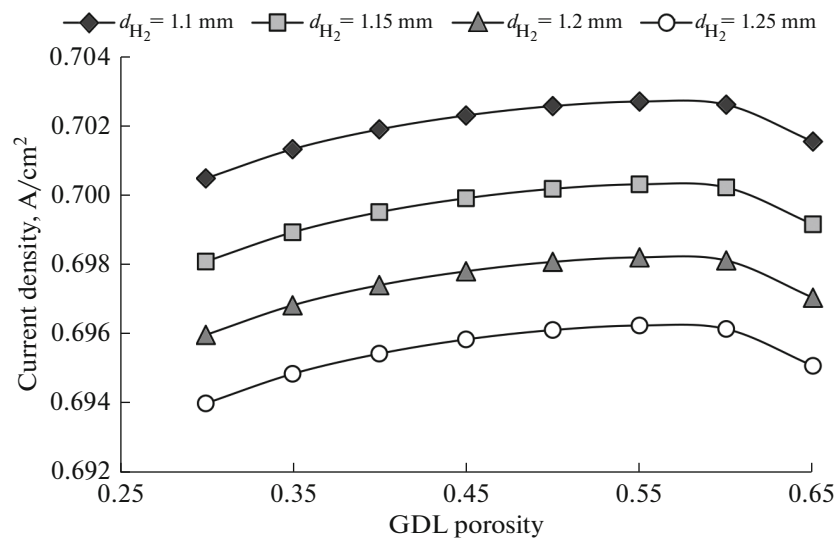
**Fig. 4.** Effect of the GDL porosity on the current density at a cell potential of 0.6 V for different hydrogen channel diameters.
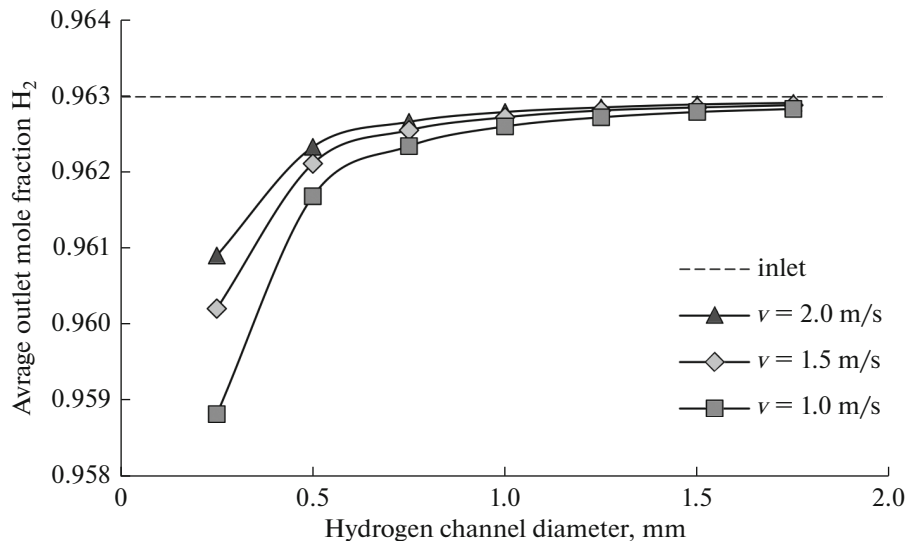


**Fig. 5.** Effect of hydrogen channel diameter on the average mole fraction of $H_2$ at the outlet of the channel.

increased for various flow velocities. The reason is the length of the channel affecting the presence of hydrogen inside the gas diffusion layer and the catalyst layer. A length of the gas diffusion layer improves the gas diffusion into the reaction sites, improving the PEM fuel cell performance.

Figure 9 shows the effect of the channel length on the average mole fraction of $H_2$ output channel at a constant channel diameter for various flow velocities. The predicted results confirm that the average outlet mole fraction of $H_2$ decreased as the channel length is increased at different flow velocities. As observed, the flow velocity 0.5 m/s, a sharp decrease in comparison of the flow velocity 1 m/s. Also, the effect of flow

velocity on the average outlet mole fraction of $H_2$ has been compared with the inlet mole fraction of $H_2$. The inlet fluid velocity ranged between about 0.5 and 1.5 m/s, which can be selected for any channel of cell based on economic rather than on physical constrains, because increased inlet fluid velocity causes significant hydrogen losses in the channel outlet of the tubular-shaped PEM fuel cell.

## CONCLUSIONS

The 3-dimensional CFD simulation of the quarter of the tubular-shaped PEM fuel according to a rigorous finite element numerical method is presented. The objective of this study was to improve the perfor-
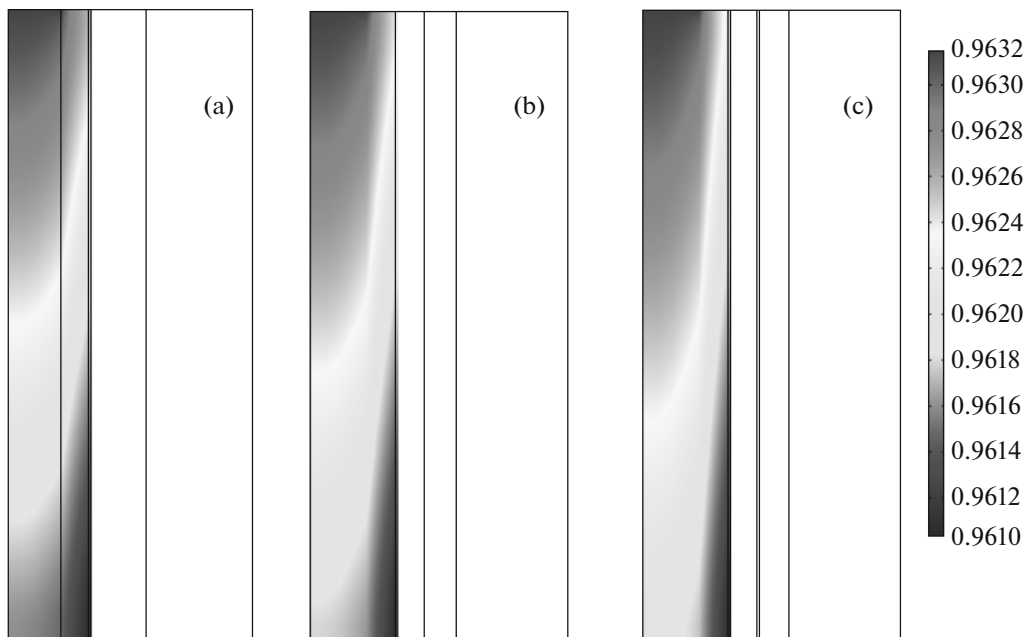
**Fig. 6.** Hydrogen molar fraction distribution in the anode side for three different velocities of gases: (a) 1, (b) 1.5, and (c) 2 m/s.
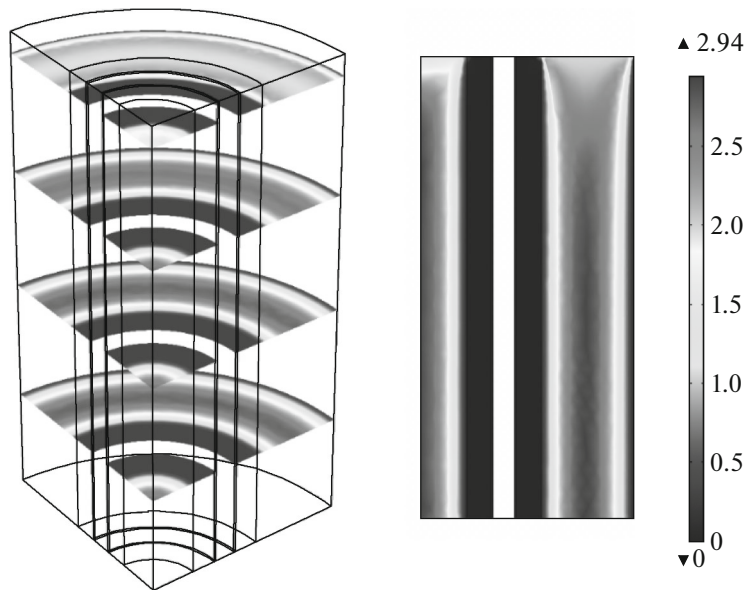


**Fig. 7.** Velocity distribution at a cell potential of 0.6 V.

mance of the tubular-shaped PEM fuel cell with the patterns co-current flow. Optimazition study using this simulated model has been applied. The computed polarization curve values are in good agreement with the measured data in the range of 0−1 A/cm². This new proposed numerical model, such as velocity distribution and species mass fractions with conventional model results shows. The simulation is conducted to investigate the effect of the hydrogen channel diameter and length on the performance of the PEM fuel cell at various flow velocities. Also to investigate their effect on the average outlet mole fraction of $H_2$ and current density in the gas diffusion layer porosity from 0.3 to 0.6. The effect of the GDL porosity on the fuel cell performance was investigated. The current density increased gradually from at porosity of 0.3 until an optimum was obtained at porosity of 0.55 at different flow velocities and hydrogen channel diameters. An
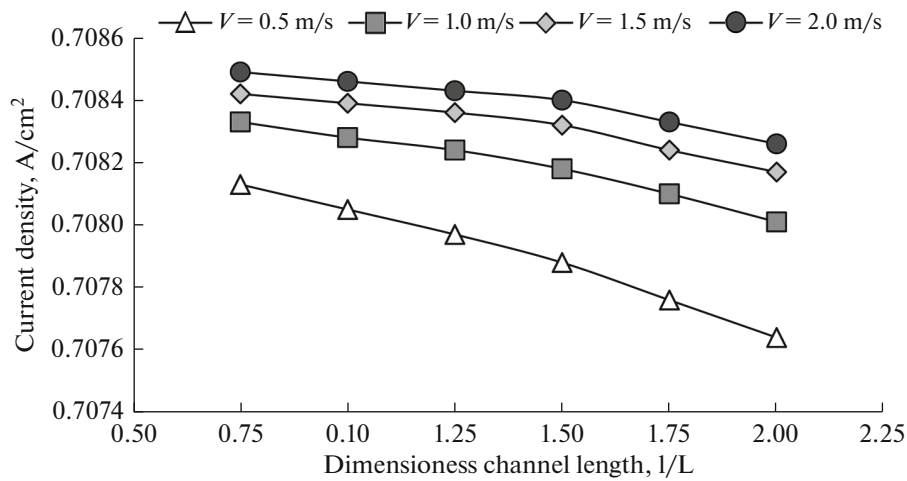
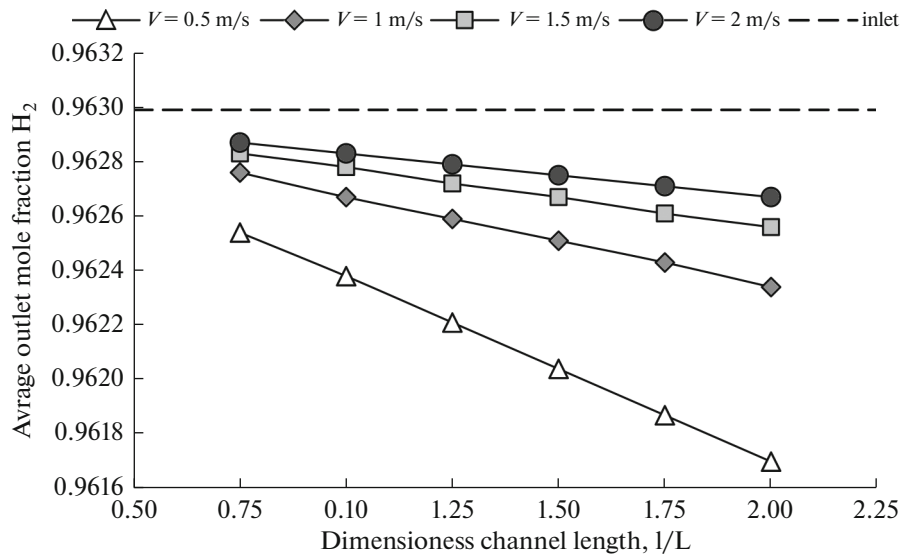**Fig. 8.** Effect of dimensionless channel length on the current density at a cell potential of 0.6 V.



**Fig. 9.** Effect of dimensionless channel length on the average mole fraction of $H_2$ at the outlet of the channel at 0.6 V.

increase in the GDL length also reduces gas reactant diffusion and subsequently reduces fuel cell performance. Furthermore, the predicted results illustrated that the reactant gases distribution is uniform at various flow velocities in the fuel cell.

### NOTATION

| | |
|---|---|
| $a_v$ | surface area, m$^2$ |
| $D_{ik}$ | Maxwell–Stefan diffusivity for the pair $i$–$k$, m$^2$/s |
| $D_{ik}^{\text{eff}}$ | Fick effective dusty gas diffusivity matrix, m$^2$/s |
| $E_{\text{eq}}$ | equilibrium thermodynamic potential |
| $F$ | Faraday's constant, 96.487 C/mol |
| $i_{v,\text{total}}$ | current density source term, A/m$^3$ |
| $i_{\text{loc}}$ | local current density |
| $i_{0,c}$ | cathodic exchange current density |
| $i_{0,a}$ | anodic exchange current density |
| $i_c$ | cathodic current density, A/m$^2$ |
| $i_a$ | anodic current density, A/m$^2$ |
| $\vec{j}_i$ | diffusion flux of the $i$th species, mol/(m$^2$ s) |
| $k_{br}$ | permeability, m$^2$ |
| $M$ | average (mixture) molecular weight, kg/mol |
| $n_m$ | number of electrons participating per electrochemical reaction |
| $p$ | pressure, Pa |
| $Q_{br}$ | source term |

| | |
|---|---|
| $R_i$ | electrochemical reactions |
| R | universal gas constant, 8.314 J/(mol K) |
| $T$ | temperature, K |
| $\vec{u}$ | velocity vector, m/s |
| $x_k$ | mole fraction of the $i$th species |
| $Y_{H_2}$ | mass fraction of hydrogen |
| $Y_{H_2}^{ref}$ | mass fraction for hydrogen at a reference |
| $Y_{O_2}$ | mass fraction of oxygen |
| $Y_{O_2}^{ref}$ | mass fraction for oxygen at a reference |
| $\alpha_{a,a}$ | anodic transfer coefficients at the anode |
| $\alpha_{a,c}$ | cathodic transfer coefficients at the anode |
| $\alpha_{c,a}$ | anodic transfer coefficients at the cathode |
| $\alpha_{c,c}$ | cathodic transfer coefficients at the cathode |
| $\varepsilon_p$ | porosity |
| $\eta_{act}$ | activation over potential, V |
| $\mu$ | overall viscosity, kg/(m s) |
| $\rho$ | overall mass density of the gas mixture, kg/m$^3$ |
| $\sigma_e$ | electrical conductivity of electrode and membrane, S/m |
| $\sigma_e^{eff}$ | effective electrical conductivity of electrode and membrane, S/m |
| $\phi$ | potential |
| $\phi_e$ | potential of electrode and membrane |
| $\omega_i$ | mass fraction of the $i$th species |

## SUBSCRIPTS AND SUPERSCRIPTS

**Subscripts**

| | |
|---|---|
| a | anode |
| act | activation |
| c | cathode |
| e | electrolyte |
| eff | effective |
| eq | equilibrium |

**Superscripts**

| | |
|---|---|
| a | anodic |
| c | cathodic |

## REFERENCES

1. Kumar, A., Mishra, S., Tripathi, B., Kumar, P., and Sharma, I.H., Aerodynamic simulation, thermal and fuel consumption analysis of hydrogen powered fuel cell vehicle, *Int. J. Veh. Struct. Syst.,* 2015, vol. 7, pp. 31–35. https://doi.org/10.4273/ijvss.7.1.06

2. Zaidi, S.M.J., Rahman, S.U., and Zaidi, H.H., R&D activities of fuel cell research at KFUPM, *Desalination,* 2007, vol. 209, pp. 319–327. https://doi.org/10.1016/j.desal.2007.04.046

3. Sadeghzadeh, K. and Salehi, M.B., Mathematical analysis of fuel cell strategic technologies development solutions in the automotive industry by the TOPSIS multi-criteria decision making method, *Int. J. Hydrogen Energy,* 2011, vol. 36, pp. 13272–13280. https://doi.org/10.1016/j.ijhydene.2010.07.064

4. Khorasani, M.R.A., Asghari, S., Mokmeli, A., Shahsamandi, M.H., and Imani, B.F., A diagnosis method for identification of the defected cell(s) in the PEM fuel cells, *Int. J. Hydrogen Energy,* 2010, vol. 35, pp. 9269–9275. https://doi.org/10.1016/j.ijhydene.2010.04.157

5. Arasti, M.R. and Moghaddam, N.B., Use of technology mapping in identification of fuel cell sub-technologies, *Int. J. Hydrogen Energy,* 2010, vol. 35, pp. 9516–9525. https://doi.org/10.1016/j.ijhydene.2010.05.071

6. Wu, H.-W., A review of recent development: Transport and performance modeling of PEM fuel cells, *Appl. Energy,* 2016, vol. 165, pp. 81–106. https://doi.org/10.1016/j.apenergy.2015.12.075

7. Manso, A.P., Marzo, F.F., Barranco, J., Garikano, X., and Mujika, M.G., Influence of geometric parameters of the flow fields on the performance of a PEM fuel cell. A review, *Int. J. Hydrogen Energy,* 2012, vol. 37, pp. 15256–15287. https://doi.org/10.1016/j.ijhydene.2012.07.076

8. Al-Baghdadi, M.A.R.S., Studying the effect of material parameters on cell performance of tubular-shaped PEM fuel cell, *Energy Convers. Manage.*, 2008, vol. 49, pp. 2986–2996. https://doi.org/10.1016/j.enconman.2008.06.018

9. Ahmadi, N., Rezazadeh, S., Mirzaee, I., and Pourmahmoud, N., Three-dimensional computational fluid dynamic analysis of the conventional PEM fuel cell and investigation of prominent gas diffusion layers effect, *J. Mech. Sci. Technol.,* 2012, vol. 26, pp. 2247–2257. https://doi.org/10.1007/s12206-012-0606-1

10. Ismail, M.S., Hughes, K.J., Ingham, D.B., Ma, L., and Pourkashanian, M., Effects of anisotropic permeability and electrical conductivity of gas diffusion layers on the performance of proton exchange membrane fuel cells, *Appl. Energy,* 2012, vol. 95, pp. 50–63. https://doi.org/10.1016/j.apenergy.2012.02.003

11. Grujicic, M., Zhao, C.L., Chittajallu, K.M., and Ochterbeck, J.M., Cathode and interdigitated air distributor geometry optimization in polymer electrolyte membrane (PEM) fuel cells, *Mater. Sci. Eng. B.,* 2004, vol. 108, pp. 241–252. https://doi.org/10.1016/j.mseb.2004.01.005

12. De Francesco, M., Arato, E., and Costa, P., Transport phenomena in membranes for PEMFC applications: An analytical approach to the calculation of membrane resistance, *J. Power Sources,* 2004, vol. 132, pp. 127–134. https://doi.org/10.1016/j.jpowsour.2004.01.044

13. Litster, S., Sinton, D., and Djilali, N., Ex situ visualization of liquid water transport in PEM fuel cell gas diffusion layers, *J. Power Sources,* 2006, vol. 154, pp. 95–105. https://doi.org/10.1016/j.jpowsour.2005.03.199

14. Dutta, S., Shimpalee, S., and Van Zee, J.W., Numerical prediction of mass-exchange between cathode and anode channels in a PEM fuel cell, *Int. J. Heat Mass*

*Transfer,* 2001, vol. 44, pp. 2029−2042. https://doi.org/10.1016/S0017-9310(00)00257-X

15. Litster, S. and McLean, G., PEM fuel cell electrodes, *J. Power Sources,* 2004, vol. 130, pp. 61−76. https://doi.org/10.1016/j.jpowsour.2003.12.055

16. Shao, Y., Yin, G., and Gao, Y., Understanding and approaches for the durability issues of Pt-based catalysts for PEM fuel cell, *J. Power Sources,* 2007, vol. 171, pp. 558−566. https://doi.org/10.1016/j.jpowsour.2007.07.004

17. Gasteiger, H.A., Panels, J.E., and Yan, S.G., Dependence of PEM fuel cell performance on catalyst loading, *J. Power Sources,* 2004, vol. 127, pp. 162−171. https://doi.org/10.1016/j.jpowsour.2003.09.013

18. Futerko, P. and Hsing, I.-M., Two-dimensional finite-element method study of the resistance of membranes in polymer electrolyte fuel cells, *Electrochim. Acta,* 2000, vol. 45, pp. 1741−1751. https://doi.org/10.1016/S0013-4686(99)00394-1

19. Rodatz, P., Büchi, F., Onder, C., and Guzzella, L., Operational aspects of a large PEFC stack under practical conditions, *J. Power Sources,* 2004, vol. 128, pp. 208−217.

20. Ahmed, D.H. and Sung, H.J., Effects of channel geometrical configuration and shoulder width on PEMFC performance at high current density, *J. Power Sources,* 2006, vol. 162, pp. 327−339.

21. Al-Baghdadi, M.A.R.S., Three-dimensional computational fluid dynamics model of a tubular-shaped PEM fuel cell, *Renewable Energy,* 2008, vol. 33, pp. 1334−1345.

22. ZareNezhad, B. and Sabzemeidani, M.M., Predicting the effect of cell geometry and fluid velocity on PEM fuel cell performance by CFD simulation, *J. Chem. Technol. Metall.*, 2015, vol. 50, pp. 176−182.

23. Al-Baghdadi, M., Three-dimensional computational fluid dynamics model of a tubular-shaped ambient air-breathing proton exchange membrane fuel cell, *Proc. Inst. Mech. Eng., Part A,* 2008, vol. 222, pp. 569−585.

24. Nguyen, P.T., Berning, T., and Djilali, N., Computational model of a PEM fuel cell with serpentine gas flow channels, *J. Power Sources,* 2004, vol. 130, pp. 149−157. https://doi.org/10.1016/j.jpowsour.2003.12.027

25. Siegel, N.P., Ellis, M.W., Nelson, D.J., and von Spakovsky, M.R., A two-dimensional computational model of a PEMFC with liquid water transport, *J. Power Sources,* 2004, vol. 128, pp. 173−184. https://doi.org/10.1016/j.jpowsour.2003.09.072

26. Wang, L., Husar, A., Zhou, T., and Liu, H., A parametric study of PEM fuel cell performances, *Int. J. Hydrogen Energy,* 2003, vol. 28, pp. 1263−1272. https://doi.org/10.1016/S0360-3199(02)00284-7